



HAL
open science

An accurate vibrational signature in halogen bonded molecular crystals

Hanine Kalout, Zahia Boubegtiten-Fezoua, François Maurel, Petra Hellwig,
Sylvie Ferlay

► **To cite this version:**

Hanine Kalout, Zahia Boubegtiten-Fezoua, François Maurel, Petra Hellwig, Sylvie Ferlay. An accurate vibrational signature in halogen bonded molecular crystals. *Physical Chemistry Chemical Physics*, 2022, 24 (24), pp.15103-15109. 10.1039/d2cp01336c . hal-03780257

HAL Id: hal-03780257

<https://cnrs.hal.science/hal-03780257>

Submitted on 20 Sep 2022

HAL is a multi-disciplinary open access archive for the deposit and dissemination of scientific research documents, whether they are published or not. The documents may come from teaching and research institutions in France or abroad, or from public or private research centers.

L'archive ouverte pluridisciplinaire **HAL**, est destinée au dépôt et à la diffusion de documents scientifiques de niveau recherche, publiés ou non, émanant des établissements d'enseignement et de recherche français ou étrangers, des laboratoires publics ou privés.

An accurate vibrational signature in halogen bonded molecular crystals

Hanine Kalout,^a Zahia Boubegtiten-Fezoua,^a François Maurel,^b Petra Hellwig,^{*a} Sylvie Ferlay^{*a}

The far infrared (FIR) and Raman fingerprints of the halogen bond in two representative 1D halogen bonded networks based on the recognition of TFIB, tetrafluorodiodobenzene, with piperazine or diazopyridine, have been accurately identified. It was demonstrated that the signature of the halogen bonding in the solid state, especially the N...I signal can be simply and directly evidenced in the far infrared region. The DFT theoretical calculations identified the N...I interaction in the molecular crystals and allows to estimate the corresponding energies and distances of the involved halogen bonds, in accordance with the crystallographic data.

Introduction

Molecular crystals are fragile entities due to their rigid morphology and periodic structure with a regular pattern. In some molecular crystals, weak intermolecular interactions such as halogen bonding (XB),^{1,2} involving noncovalent interactions between electron-deficient halogen atom X (Lewis acid, halogen bond donor) and electron-rich molecule D (Lewis base, halogen bond acceptor), are encountered. The almost linear directionality of this non-covalent interaction makes it a promising tool for the design and tuning of new functional molecular crystals^{3,4,5} and among them, inherent mechanical properties. For example, soft crystals, a subcategory of molecular crystals, can present macroscopic deformations, under the influence of different external stimuli, such as pressure, temperature, humidity and light, for example.⁶ This specificity may find applications in miniaturized optoelectronic devices, optical waveguides, sensors, biomimetics, explosives, etc.^{1,7} Among soft crystals, elastic⁸ and plastic crystals⁹ are generally built from weakly interacting molecules, using weak supramolecular interactions. In such crystals, the role of the weak interactions is crucial and deserve an in-depth spectroscopic investigation.

Spectroscopic approaches provide reliable and fast access to information that contributes to the understanding of strong and weak interactions between different components of molecular crystals.¹⁰ Combined spectroscopies like solid state NMR and vibrational spectroscopy for example, may be useful for the investigation of non-covalent interactions in molecular networks¹¹

and also for the comprehension of the intrinsically mechanical properties of molecular compounds.

Since few decades, there were several reports of crystalline compounds involving halogen atoms, that have been studied by infrared and Raman spectroscopy.^{1-5,12,13,14} Till now, only few reports focus on halogen bonds of molecular crystals in the solid-state, and their classical spectroscopic signature.^{1-3,5,15,16} Though the halogen bond spectroscopic signature has been relatively well-known for compounds in solution,^{17,18,19,20} the study in the solid state is still at its infancy. For molecular compounds in the solid state, to the best of our knowledge, the Raman and far IR spectral signatures of the halogen bond have been recently briefly explored for one molecular network²¹ or for iodine-chlorine interhalides salts.²² It seems that the spectroscopic signature of the halogen bond has an important interest in the understanding of these interactions that accounts for their mechanical properties (plastic or elastic, for example).

In the present study, we describe the far infrared (FIR) and the Raman spectral features of simple XB infinite molecular networks and demonstrate that the halogen bonding, in the solid state, can be simply and directly monitored.

Results and discussion

Structure of the obtained networks

We choose two representative halogen bonded crystalline networks based on the ditopic C₆F₄I₂ (TFIB, tetrafluorodiodobenzene)²³ building block, that is well-known to be involved in strong N...I halogen bonds, as already shown in recently reported networks.^{24,25,26} We studied the combination of this building block with a non-aromatic amine (Piperazine, adopting a chair like feature), behaving as a X bond acceptor and an aromatic X-bond acceptor (Azopyridine), as shown in Figure 1. In the solid state, the formed 1D X bonded networks have been analysed in the 300 to 50 cm⁻¹ spectral

^a Université de Strasbourg-CNRS, UMR 7140, F-67000 Strasbourg, France. Email : ferlay@unistra.fr, hellwig@unistra.fr

^b Université de Paris, ITODYS, CNRS, F-75006 Paris, France.

Electronic Supplementary Information (ESI) available: PXRD diagrams for **1** and **2**, temperature dependence the halogen bonding band of **1** in the 100-50 cm⁻¹ spectral range, crystallographic table, geometrical parameters for DFT calculations and calculated FIR and Raman spectra for **1** and **2**.

. See DOI: 10.1039/x0xx00000x

region, by using both FIR and Raman spectroscopies. To corroborate and provide valuable insight into the peak assignment found in the experimental results, we also performed density functional theory (DFT) calculations.

The combination of TFIB with either piperazine or diAzopyridine leads to a 1D X bonded network, due to the directional character of the N...I interaction, as shown in Figure 1. The crystal structures of compound **1** (TFIB combined with piperazine, CCDC Refcode: DIVCUH, we also performed structure analysis at 100K, see Table S1 in the ESI)²⁷ and compound **2** (TFIB combined with azopyridine, CCDC Refcode: BULKEA²⁸) have been already reported in the literature. Crystals of **1** and **2** have been obtained in self-assembly conditions (see experimental part) and the purity of their corresponding polycrystalline phase has been checked using powder X-ray diffraction (PXRD) (Figure S1 in the ESI). In both cases, a 1D compound is formed through the formation of halogen bonds, between the nitrogen and iodine atoms. At the temperature of the crystallographic measurements (see Table 1), the N...I distance in **1**, is reported to be 2.842 (5) Å²⁷ (observed at 2.845(3) Å at 100K) and close to 2.880(6) Å²⁸ in **2**. The θ_{INC} values are equal to 176.89°²⁷ for **1** (measured to be 177.06° at 100K) and 179.48°²⁸ for **2**.

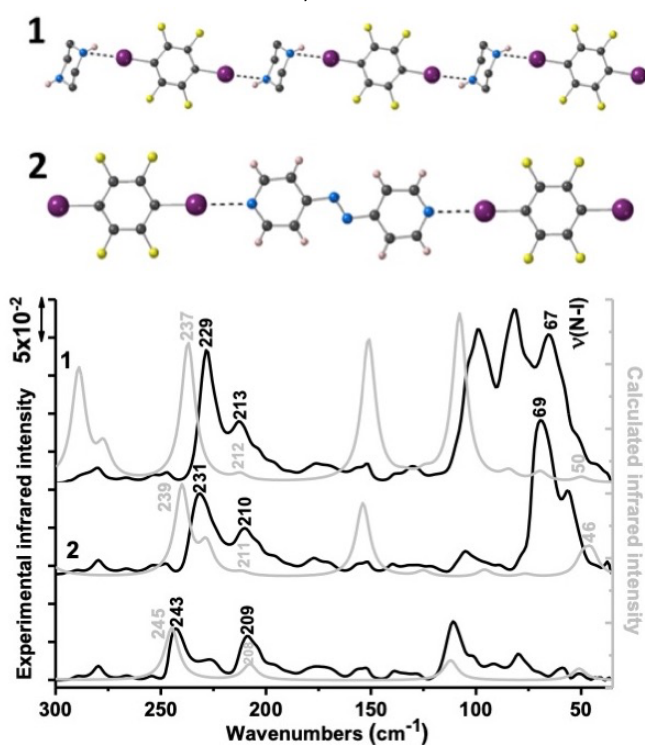


Figure 1: Schematic representation of studied 1D molecular networks, **1** and **2** (top). Colors are as follows: C, grey; F, yellow; H, pink; I, magenta; N, blue. Experimental ATR-FIR spectra of TFIB donor (bottom) and related crystals **1** (top) and **2** (middle) (in black), compared with the corresponding simulated infrared spectra (in grey) using the TFBI..Piperazine and TFBI..Azopyridine models for **1** and **2** respectively. The experimental spectra are recorded on powdered crystalline samples. The calculated spectral intensities for **1** and **2** respectively are provided in Table 2.

Spectroscopic investigations

For both compounds **1** and **2**, the signals between 300 and 50 cm⁻¹, were analysed in the solid state, on powdered crystalline samples, at RT, using FIR and Raman spectroscopies. The different bands obtained for TFIB and crystals **1** and **2** were tentatively assigned to vibrational modes attributed previously to similar halogen-bonded crystals involving haloperfluoroaromatic donors, as seen in Table 2.²¹ As shown in Figures 1 and 2A, the fingerprints of the C-I (stretching and bending) vibrations are shown for TFIB in the low frequency range, and they have been compared to the vibrations observed for compounds involving TFIB.²¹

In the ATR-FIR spectrum of pure TFIB (see black curve in the bottom of Figure 1), two bands are found at 209 and 243 cm⁻¹, which correspond to C-I bending vibrations (at 209 cm⁻¹) and to C-I stretching vibration (at 243 cm⁻¹). Two bands at 142 and 156 cm⁻¹, tentatively assigned to the C-I bending (142 cm⁻¹) and C-I stretching (156 cm⁻¹) vibrations, are observed in the Raman spectrum of TFIB (see black curve in the bottom of Figure 2A). Upon involvement of TFIB in intermolecular halogen bonds, a redshift of around 13 cm⁻¹ was observed for the $\nu_{\text{C-I}}$ vibration, whereas the $\delta_{\text{C-I}}$ mode was shown to shift to higher wavenumbers (blue shift) by approximately 11 cm⁻¹ (values averaged from FIR and Raman data of both crystals networks **1** and **2**) (see black curves in the top and the middle of Figures 1-2A and Table 2). A similar redshift for $\nu_{\text{C-I}}$ vibration was previously reported²¹ for the halogen-bonded complex of pyridine and iodopentafluorobenzene (IPFB) and can be correlated to the weakening and lengthening of the C-I bonds²⁹ in the XB 1D network. Furthermore, the experimental FIR and Raman intensities of C-I stretching band of TFIB involved in crystals network are two orders of magnitude higher when directly compared to the same band in pure TFIB (see black curves in Figures 1-2A). An explanation of the increase of intensity occurring upon halogen-bond formation may be based on the charge-transfer character of the halogen bond and also on its partially covalent nature.³⁰ We note, however, that there are no changes in the intensity of C-I bending vibrational band of TFIB involved in halogen bond. In addition, the spectral changes for the C-I stretching band differ for both crystals networks, with more changes observed in case of crystal **1** with piperazine as halogen-bond acceptor molecule. These results confirmed the features that such as red-shift and increased intensity of the C-I stretching band are indicative of the successful formation of the halogen bond involving TFIB.

In the spectral range between 100 and 50 cm⁻¹, infrared bands at 67 cm⁻¹ for **1** and 69 cm⁻¹ for **2** (see black curves in the top and the middle of Figure 1) were detected and assigned to N...I stretching vibration from the respective halogen-bonded complexes. The Raman spectra measured for crystals of **1** and **2** at low frequency also exhibit bands at 61 and 74 cm⁻¹, respectively, corresponding to the N...I stretching vibration (see black curves in the top and the middle of Figure 2A). In addition, this molecular vibration band, that is assigned above to the halogen bond, is intense despite of its nature.

Investigation of the thermal behavior of halogen bonded complexes provides information about their relative stabilities,

which is important for their applications. Few data related to the influence of temperature on the halogen bond are available,^{12,31} and the halogen bond length is strongly dependent on temperature. For this reason, we decided to study the halogen bond that includes the N...I stretching vibration as function of temperature in the 20-70 °C range using Raman spectroscopy on crystals **1** and **2** (see Figure S2 and Figure 2B, respectively).

A shift of ν_{N-I} mode of about 3 cm^{-1} towards lower wavenumbers was shown when the temperature is increasing for crystal **2** (see Figure 2B), revealing a weakening of the halogen bonding. This change undergoing a redshift of ν_{N-I} in crystal **2** was found to be fully reversible. In case of crystal **1**, the shift is not observed for the ν_{N-I} mode (see the Figure S2) reflecting a different nature of the halogen bonding, as shown by its shorter distance.

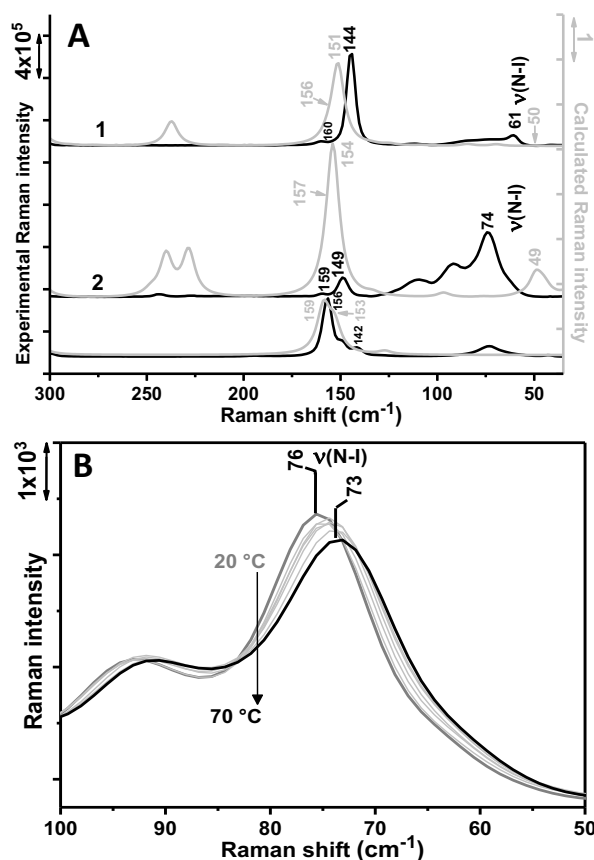


Figure 2: A) Experimental Raman spectra of TFIB (bottom), crystals **1** (top) and **2** (middle) (in black) compared to the corresponding simulated Raman spectra (in grey), using the TFIB..Piperazine and TFIB..Azopyridine models for **1** and **2** respectively. The experimental spectra are recorded on powdered crystalline samples. The calculated spectral intensities are given in Table 2. B) the temperature dependence of the halogen bonding mode (ν_{N-I}) of **2** from 20 to 70 °C in the 100-50 cm^{-1} spectral range.

Modeling

In order to model the behavior of the crystalline extended compounds **1** and **2**, both bimolecular (TFIB..Piperazine or TFIB..Azopyridine) and trimolecular “compounds” (TFIB..(Piperazine)₂ or TFIB..(Azopyridine)₂) involving one or two Lewis base have been investigated. In the literature, ab initio calculations have been successfully used to study the

intermolecular interaction energies of halogen bonded complex of pyridine with $\text{C}_6\text{F}_5\text{I}$ ²⁹. In addition, very recently, the electronic structural origin of the THz and IR spectral changes occurring upon halogen-bonding formation has been reported for the complexes of $\text{C}_6\text{F}_5\text{I}$ formed with other halogen-bond accepting molecules.^{30,32}

In the current work, DFT calculations involving complexes of TFIB with either piperazine or 4,4'-azopyridine have been performed in the gas phase (see the experimental part for the detailed methodology). The optimized geometries for the halogen-bonded complexes of TFIB with piperazine and 4,4'-azopyridine are shown in Figure 3 and the relevant structural data for the monomers and for the complexes are reported in Table S2 (see the ESI). The N...I halogen-bond distances are found to be equal to 2.866 Å and 2.913 Å for **1** and **2** in trimolecular complexes TFIB..(Piperazine)₂ and TFIB..(Azopyridine)₂ respectively, both values are in good agreement with the experimental data provided by X-Ray diffraction. Furthermore, the halogen-bonded complexes exhibit a nearly linear geometry, θ_{INC} between 175.9 and 178.9° (see Table S2 in the ESI).

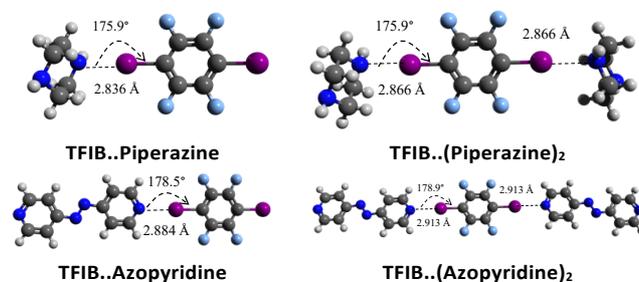


Figure 3. Equilibrium geometries for the halogen-compounds of TFIB with piperazine ((analogue to **1**, TFIB..Piperazine and TFIB..(Piperazine)₂) (top) and with 4,4'-Azopyridine (analogue to **2** TFIB..Azopyridine and TFIB..(Azopyridine)₂) (bottom)).

In addition, the interaction energy of the N...I interaction in the bi and trimolecular compounds was estimated between -10.3 and -13.9 kcal/mol and are summarized in Table 1. Concerning the predicted interaction energies, they appear to be a little bit higher than the intermolecular interaction energies calculated for $\text{C}_6\text{F}_5\text{I}$ -pyridine compound.²⁹ For the XB interaction N...I, the $d_{N...I}$ distances are in accordance with values obtained experimentally using X-Ray diffraction. Indeed, due to a weaker interaction for **2**, the observed N...I distance is a little longer than the distance observed for **1**.

| | Exp $d_{N...I}$ (100K) Å | Calc $d_{N...I}$ (0 K) Å | Calc $\Delta E_{\text{interaction}}$ (kcal/mol) |
|----------|----------------------------------|--------------------------------|--|
| 1 | TFIB..Piperazine | 2.866 | -13.8 |
| | TFIB..(Piperazine) ₂ | 2.866 | -13.9 |
| 2 | TFIB..Azopyridine | 2.913 | -10.3 |
| | TFIB..(Azopyridine) ₂ | 2.913 | -10.5 |

Table 1: Comparison of the experimental and calculated values of $d_{N...I}$ distances for **1** and **2**, as well as an estimation of the N...I interaction energy of involved XB.

A detailed analysis for the experimental (at 294K) and simulated FIR and Raman spectra (at 0K) has been performed and a comparison

of the experimental vibrational frequencies with the computed values is shown in Figures 1-2A and Table 2. There are many similarities in the spectral features obtained from the experimental and the spectra modelled in the gas phase for TFBI donor molecule and crystals **1** and **2**. The total number of bands is comparable; however, some additional features are seen in the experimental solid-state spectra. The direct comparison of the signal intensities shows only a weak correlation likely due to the lack of crystal packing in the cluster-based DFT method. Here, no scaling was applied to the calculated spectral intensities of TFIB and crystals **1** and **2** in Figures 1-2A. We increased the intensities of the bands of the calculated infrared and Raman spectra by a factor of 5 to show the positions of the low intensity bands including the halogen bonding band (see Figures 1-2A). The real calculated spectral intensities are provided in Table 2.

The performed calculations also evidenced the weakness of the C-I bond after the formation of the crystalline network, by a decrease of the frequency of the stretching vibration ν_{C-I} in Raman spectra from 159 (for TFIB) to 151 cm^{-1} for **1** and to 149 cm^{-1} for **2** (see grey curves in the Figure 2A and Table 2). An analogue frequency redshift of the ν_{C-I} vibration is observed in the experimental Raman spectra of TFIB..Piperazine and TFIB..Azopyridine (12 and 7 cm^{-1}) (see Table 2 and Figure 2A). Additionally, upon modelling the XB interaction in the gas phase, we noted a decrease of the frequency of the stretching vibration ν_{C-I} from 159 cm^{-1} in TFIB to 151 cm^{-1} and 149 cm^{-1} in TFIB..Piperazine and TFIB..(Piperazine)₂ Raman spectra, respectively (see Table 2 and Figures 2A and S3). A similar trend is observed from the calculated infrared spectra, with a redshift of 15 cm^{-1} seen for the ν_{C-I} vibration upon formation of the trimolecular compound (TFIB..(Piperazine)₂) (see Table 2 and Figures 1 and S3). This change evidences again the weakness of the C-I bond after the N...I halogen-bond formation in the molecular crystals. The same effect is observed experimentally in the infrared spectral range on ν_{C-I} (redshift of 14 cm^{-1}) of TFIB involved in TFIB..Piperazine crystal network (see Table 2 and Figure 1). The ν_{C-I} mode is also predicted to undergo a pronounced Raman and IR intensities increase in crystals **1** and **2**, thus following the experimental observations.

A very weak intensity band is calculated at 153 cm^{-1} and 208 cm^{-1} in the respective Raman and FIR spectra of TFIB and assigned to the C-I bending (δ_{C-I}) vibration (see Table 2 and Figures 1-2A). The position of this band is slightly modified upon interaction of TFIB with piperazine halogen-bond acceptor molecule (blueshift of 5 cm^{-1}) (see Table 2 and Figures 1-2A and S3). Similar changes are found for the δ_{C-I} band in IR and Raman spectra of TFIB-Azopyridine halogen-bonded compounds (blueshift of 5 cm^{-1}) (see Table 2 and Figures 1-2A and S4). The calculated Raman and IR intensities of the C-I bending mode of TFBI are changed marginally upon halogen bond formation with piperazine and azopyridine acceptor molecules. The trends observed for δ_{C-I} in the experimental data are well reproduced.

| Stretching C-I | | |
|---|----------------|-------------------------|
| | ν_{C-I} | |
| | Raman | IR (cm^{-1}) |
| Experimental | | |
| TFIB | 156 | 243 |
| 1 | 144 | 229 |
| 2 | 149 | 231 |
| Calculated | | |
| TFBI | 159 (4) | 245 (2) |
| 1 TFBI..Piperazine | 151 (23) | 237 (11) |
| 1 TFBI..(Piperazine) ₂ | 149 (56) | 230 (38) |
| 2 TFBI..Azopyridine | 154 (8) | 239 (10) |
| 2 TFBI..(Azopyridine) ₂ | 151 (124) | 236 (30) |
| Bending C-I | | |
| | δ_{C-I} | |
| | Raman | IR (cm^{-1}) |
| Experimental | | |
| TFIB | 142 | 209 |
| 1 | 160 | 213 |
| 2 | 159 | 210 |
| Calculated | | |
| TFBI | 153 (2) | 208 (0.5) |
| 1 TFBI..Piperazine | 156 (1.5) | 212 (0.5) |
| 1 TFBI..(Piperazine) ₂ | 157 (1) | 216 (0.7) |
| 2 TFBI..Azopyridine | 157 (2.5) | 211 (0.4) |
| 2 TFBI..(Azopyridine) ₂ | 159 (3) | 215 (0.4) |
| Stretching N-I (XB) | | |
| | ν_{N-I} | |
| | Raman | IR (cm^{-1}) |
| Experimental | | |
| TFIB | - | - |
| 1 | 61 | 67 |
| 2 | 74 | 69 |
| Calculated | | |
| TFBI | - | - |
| 1 TFBI..Piperazine | 50(0.01) | 50(1.9) |
| 1 TFBI..(Piperazine) ₂ | 55(0.09) | 48(3.7) |
| 2 TFBI..Azopyridine | 49(0.6) | 46(12) |
| 2 TFBI..(Azopyridine) ₂ | 38(1.5) | 51(39) |

Table 2: Overview on the assignments of the TFIB, **1** and **2** vibrations in the spectral region from 300 to 50 cm^{-1} . Comparison of the experimental vibrational frequencies (Raman and FIR) with computed frequencies (Intensities) for the fundamentals (ν : stretching and δ : deformation in cm^{-1}). Intensities are given in brackets for the calculated values.

The DFT simulations also allow to highlight the N...I stretching vibration in the IR (Raman) spectra for both **1** and **2** at 50 (50) and 48 (55) cm^{-1} for TFBI..(Piperazine) and TFBI..(Piperazine)₂, respectively, and also at 46 (49) and 51 (38) cm^{-1} for TFBI..(Azopyridine) and TFBI..(Azopyridine)₂, respectively (see Table 2 and Figures 1-2A and S3-4). The ν_{N-I} computed frequencies are smaller than the observed values (see Table 2 and Figures 1-2A). The weak agreement between the gas phase calculated and solid state measured N...I wavenumbers in the halogen bonded cocrystals is probably due to the different environmental effects that are known to exist in the co-crystals, as crystal packing effects.³³ This could be due

also to the used finite model that ignore the anharmonic effect from the calculations based on the numerical differentiation.

Experimental

Synthetic procedures

Synthesis of the crystalline compounds was performed by slightly modifying the already reported procedures.

1: 1,4-diiodotetrafluorobenzene + piperazine²⁷

1,4-diiodotetrafluorobenzene ($5,226 \times 10^{-5}$ mol, 21 mg) was dissolved in 3 mL dichloromethane and piperazine ($1,056 \times 10^{-4}$ mol; 9,1 mg) was dissolved in 6 mL CH_2Cl_2 . The resulting colourless solutions were mixed together without stirring. After two days, colourless crystals were obtained from the filtrate, dried in air and stored.

2: 1,4-diiodotetrafluorobenzene + 44'-azopyridine²⁸

1,4-diiodotetrafluorobenzene ($2,488 \times 10^{-5}$ mol, 10 mg) was dissolved in 3 mL CH_2Cl_2 and 44'-azopyridine ($4,886 \times 10^{-5}$ mol; 9 mg) was dissolved in 6 mL CH_2Cl_2 . The resulting solutions were mixed together without stirring. After two days, orange crystals were obtained from the filtrate, dried in air and stored.

Crystal structure confirmation

Powder X-ray diffraction (PXRD) provides information on phase composition, chemical composition and the crystal structure of the analysed materials. PXRD diagrams were collected on a Bruker D8 diffractometer using a monochromatic $\text{Cu-K}\alpha$ radiation, with a scanning range between 3° and 40° (2θ), with a step size of 0.008° and time per step of 0.4s.

Spectroscopic investigations

Far-Infrared Spectroscopy

The Far-infrared (FIR) data were obtained with a globar light source for the spectral range $700\text{--}50\text{ cm}^{-1}$ with a scan velocity of 2.5 kHz, on the pure polycrystalline samples (TFIB, 1 and 2). The FIR spectra were recorded with the help of a Vertex 70 FT-IR spectrometer (Bruker, Germany) in the attenuated total reflection mode (ATR) (Harrick crystal, Diamond Prism). A Si beamsplitter and a room temperature deuterated triglycine sulfate (RT-dTGS) detector were used. Five spectra with a resolution of 4 cm^{-1} (128 co-added scans) were averaged for each sample. The spectrometer was purged with dry air to avoid the contributions from humidity in the spectra. The ATR-FIR spectra of TFIB, and the crystal samples were performed from powders.

ATR-FIR spectra were recorded with the Opus software from Bruker (Opus. 6.0) and analyzed with Origin program (OriginLab. 8.5). The baseline correction was applied for each sample spectrum.

Confocal Raman spectroscopy

Raman scattering instrumentation:

Confocal Raman microscope system was used for Raman scattering measurements, which is composed of an inVia Renishaw spectrometer (grating: 1200 lines/mm) and a TE-cooled charge-coupled device (CCD) as detector.

The spectral resolution of the spectrometer is 1 cm^{-1} . Elastically scattered light was removed with an edge filter. An argon STELLAR laser source (30 mW/514.5 nm) in a backscatter configuration was focused on the sample using a 50X/0.75 NA dipping microscope objective (Leica). The spot of the laser used in the Raman experiments had a diameter of $0.67\text{ }\mu\text{m}$.

Raman measurements:

The Raman spectra of the polycrystalline samples (TFIB, 1 and 2) were measured on powdered samples in a confocal mode with a laser of 12 mW (the laser power was measured at the exit of the microscope objective). Exposure time of the measurements was 10 s. 10 accumulations were made to obtain Raman spectra (from 0 to 3200 cm^{-1}) with an optimal signal to noise ratio. It should be also mentioned that all presented Raman spectra have been baseline corrected. Raman spectra were recorded with the Wire software from Renishaw (Wire. 3.4) and analyzed with Origin program (OriginLab. 8.5).

The temperature-dependent Raman measurement of **1** and **2** as powders have been obtained with a home cell made of two CaF_2 windows, few crystals of each compound have been deposited on a window that was covered with another one. The windows were placed in the metallic support of the cell and then it was placed in a confocal mode Raman spectrometer ($20\times/0.40$ NA dipping microscope objective (Leica)) and connected also to the thermostatic bath to control the temperature. The Raman spectra were recorded between 20 and $70\text{ }^\circ\text{C}$ by a step of 10°C and the samples were equilibrated for 10 minutes at the respective temperature before data acquisition. The spectra of the crystals networks **1** and **2** were measured as powders with a laser excitation of 514 nm and 12 mW laser power. Exposure time of the measurements was 10 s. 10 accumulations were made to obtain spectra of the compounds (from 0 to 3200 cm^{-1}) with an optimal signal to noise ratio.

Computational Details: DFT calculations

In the computational part we studied the effect of the complexation through halogen bonding on the spectroscopic behavior of the TFBI. Therefore, we studied the molecular complexes formed between TFBI with one or two Lewis base such as Piperazine ou Azopyridine. These molecular models, **1** TFBI..Piperazine, **1** TFBI..(Piperazine)₂, **2** TFBI..Azopyridine or **2** TFBI..(Azopyridine)₂ are supposed to reproduce the complexes **1** and **2**, respectively.

Therefore equilibrium geometries and harmonic vibrational frequencies of TFIB, piperazine, azopyridine and complexes **1** and **2** were obtained from DFT calculations using the PBE0 functional.³⁴ Standard pople basis set 6-311G(d,p) were used for

hydrogen, carbon, nitrogen, and fluorine atoms, whereas for iodine the LanL2DZ basis sets taken from the EMSL basis Set Exchange Library³⁵ was used.

All the calculations were performed using *Gaussian 09*³⁶ and the molecular structures were confirmed as real minima of the potential energy surface on the basis of their harmonic vibrational frequencies, which showed positive force constants for all normal modes. Basis set superposition error (BSSE)^{37,38} in the complexes was corrected by means of the counterpoise (CP) scheme.³⁹

Previous studies^{40,41} have shown that dispersion interactions can play a significant role in the Halogen bonds interaction. Therefore, we compare the results obtained using several different functionals, *i.e.* PBE0, PBE0 including empirical dispersion term GD3 (PBE0-GD3)⁴² and the hybrid meta exchange-correlation functional M06.⁴³ As revealed by the data gathered in the Tables S2 and S3, the results are similar whatever the functional used for the geometries and the vibrational properties of the calculated complexes. Considering these results, we discussed only the PBE0 calculations in the text.

Conclusions

We applied FIR and Raman spectroscopies and DFT calculations to characterize two types of 1D halogen bonded networks involving the linear ditopic XB donor C₆F₄I₂ (TFIB, tetrafluorodiodobenzene) and a nonaromatic (piperazine, compound **1**) and an aromatic (diazobenzene, compound **2**) in the crystalline state. For the first time, the spectroscopic fingerprint of the halogen bond (N...I interaction) was evidenced for both compounds in the 100 to 40 cm⁻¹ spectral region. The

halogen bond formation was directly detected in the experimental and the simulated FIR and Raman spectra via the redshift of the C-I stretching vibrations, and the blueshift of the C-I bending vibrations. The DFT theoretical calculations confirmed the occurrence of the halogen bonds in the obtained crystals in gas phase and estimated the N...I halogen bond energy to be -13.8 and -10.3 kcal/mol for **1** and **2** respectively. The new fingerprint of the N... I interaction here reported contributes to the deep understanding of weak molecular interactions of halogen bonding governing the formation of crystals and also their expected properties, like the mechanical properties, for example. This unique fingerprint may also be of interest for a large class of materials.

Author Contributions

The authors contributed equally to the presented work

Conflicts of interest

There are no conflicts to declare.

Acknowledgements

Financial support from the University of Strasbourg and the CNRS is acknowledged. Nathalie Gruber (UMR 7140) is acknowledged for resolving the structure of **1** at 100K.

Notes and references

- 1 G. R. Desiraju, P. S. Ho, L. Kloo, A. C. Legon, R. Marquardt, P. Metrangolo, P. Politzer, G. Resnati, K. Rissanen, Definition of the Halogen Bond (IUPAC Recommendations 2013) *Pure Appl. Chem.* 2013, **85**, 1711-1713.
- 2 G. Cavallo, P. Metrangolo, R. Milani, T. Pilati, A. Priimagi, G. Resnati, G. Terraneo, The Halogen Bond. *Chem. Rev.* 2016, **116**, 2478-2601.
- 3 K. Rissanen, Halogen bonded supramolecular complexes and networks *CrystEngComm*, 2008, **10**, 1107-1113.
- 4 A. Mukherjee, S. Tothadi, G. R. Desiraju, Halogen Bonds in Crystal Engineering: Like Hydrogen Bonds yet Different. *Acc. Chem. Res.* 2014, **47**, 2514-2524.
- 5 M. Saccone, L. Catalano, Halogen Bonding Beyond Crystals in Materials Science. *J. Phys. Chem. B.* 2019, **123**, 9281-9290.
- 6 G. Soumyajit, M. K. Mishra, Elastic molecular crystals: From serendipity to design to applications. *Cryst. Growth Des.*, 2021, **21**, 2566-2580.
- 7 M. Pisacic, I. Biljan, I. Kodrin, N. Popov, Z. Soldin, M. Dakovic, Elucidating the origins of a range of diverse flexible responses in crystalline coordination polymers. *Chem. Mater.*, 2021, **33**, 3660-3668.
- 8 G. Soumyajit, M. K. Mishra, Elastic molecular crystals: From serendipity to design to applications. *Cryst. Growth Des.* 2021, **21**, 2566-2580.
- 9 A. Mondal, B. Bhattacharya, S. Das, S. Bhunia, R. Chowdhury, S. Dey, C. M. Reddy, Metal-like ductility in organic plastic crystals: Role of molecular shape and dihydrogen bonding interactions in aminoboranes. *Angew. Chem. Int. Ed.* 2020, **59**, 10971-10980.
- 10 Y. El Khoury, P. Hellwig, Far infrared spectroscopy of hydrogen bonding collective motions in complex molecular systems. *Chem. Commun.*, 2017, **53**, 8389-8399.
- 11 V. Kumar, Y. Xu, C. Leroy, D. L. Bryce, Direct investigation of chalcogen bonds by multinuclear solid-state magnetic resonance and vibrational spectroscopy. *Phys.Chem.Chem.Phys.*, 2020, **22**, 3817-3824.
- 12 M. H. Abraham, F.W. Parrett, Low frequency infrared and Raman spectra of the N,N,N',N'-tetramethyl- ethylenediamine adducts of the Group II b dihalides *Can. J. Chem* 1970, **48**, 181-184.
- 13 A. Anderson, B. Andrews, B. H Torrie, Raman and Infrared studies of the lattice vibrations of some halogen derivatives of methane *J. Chim. Phys.*, 1985, **82**, 99-109.
- 14 R. G. Niemann, A. G. Kontos, D. Palles, E. I. Kamitsos, A. Kaltzoglou, F. Brivio, P. Falaras, P. J. Cameron Halogen Effects on Ordering and Bonding of CH₃NH₃⁺ in CH₃NH₃PbX₃ (X = Cl, Br, I) Hybrid

- Perovskites: A Vibrational Spectroscopic Study *J. Phys. Chem. C* 2016, **120**, 2509-2519.
- 15 M. K. Panda, S. Ghosh, N. Yasuda, T. Moriwaki, G. D. Mukherjee, C. M. Reddy, P. Naumov, spatially resolved analysis of short-range structure perturbations in a plastically bent molecular crystal. *Nat. Chem.*, 2015, **7**, 65-72.
 - 16 L. O. Alimi, P. Lama, V. J. Smith, L. Barbour, Hand-twistable Plastically Deformable Crystals of a Rigid Small Organic Molecule. *Chem. Commun.*, 2018, **54**, 2994-2997.
 - 17 R. Glaser, N. Chen, H. Wu, N. Knotts, M. Kaupp, ¹³C NMR Study of Halogen Bonding of Haloarenes: Measurements of Solvent Effects and Theoretical Analysis *J. Am. Chem. Soc.* 2004, **126**, 13, 4412-4419.
 - 18 D. Hauchecorne, R. Szostak, W. A. Herrebout, B. J. van der Veken, C-X...O Halogen Bonding: Interactions of Trifluoromethyl Halides with Dimethyl Ether *ChemPhysChem.*, 2009, **10**, 2105-2115.
 - 19 N. Nagels, D. Hauchecorne, W. A. Herrebout, Exploring the C-X... π Halogen Bonding Motif: An Infrared and Raman Study of the Complexes of CF₃X (X = Cl, Br and I) with the Aromatic Model Compounds Benzene and Toluene *Molecules*, 2013, **18**, 6829-6851.
 - 20 T. A. Bramlett, A. J. Matzger, Halogen Bonding Propensity in Solution: Direct Observation and Computational Prediction *Chem. Eur. J.* 2021, **27**, 15472-15478.
 - 21 V. Vasylyeva, L. Catalano, C. Nervi, R. Gobetto, P. Metrangolo, G. Resnati, Characteristic redshift and intensity enhancement as far-IR fingerprints of the halogen bond involving aromatic donors. *CrystEngComm.*, 2016, **18**, 2247-2250.
 - 22 M. S. Abdelbassit, O. J. Curnow, M. K. Dixon, M. R. Waterland, The Binary Iodine-Chlorine Octahalide Series [InCl₈-n]₂ *Chem. Eur. J.*, 2019, **25**, 11650-11658.
 - 23 R. Bailey Walsh, C.W. Padgett, P. Metrangolo, G. Resnati, T.W. Hanks, W.T. Pennington, Crystal Engineering through Halogen Bonding: Complexes of Nitrogen Heterocycles with Organic Iodides. *Cryst. Growth Des.*, 2001, **1**, 165-175.
 - 24 A. Forni, P. Metrangolo, T. Pilati and G. Resnati, Halogen Bond Distance as a Function of Temperature. *Cryst. Growth Des.*, 2004, **4**, 291-295.
 - 25 M. C. Pfrunder, A. J. Brock, J. J. Brown, A. Grosjean, J. Ward, J. C. McMurtrie, J. K. Clegg, A three-dimensional cubic halogen-bonded network. *Chem. Commun.*, 2018, **54**, 3974-3976.
 - 26 L. Happonen, J. M. Rautiainen, A. Valkone, Halogen Bonding between Thiocarbonyl Compounds and 1,2- and 1,4-Diodotetrafluorobenzenes. *Cryst. Growth Des.*, 2021, **21**, 3409-3419.
 - 27 D. Cinčić, T. Friščić, W. Jones, Isostructural Materials Achieved by Using Structurally Equivalent Donors and Acceptors in Halogen-Bonded Cocrystals. *Chem. Eur. J.* 2008, **14**, 747-753.
 - 28 P. Ravat, S. Seetha Lekshmi, S. N. Biswas, P. Nandy, S. Varughese, Equivalence of Ethylene and Azo-Bridges in the Modular Design of Molecular Complexes: Role of Weak Interactions. *Cryst. Growth Des.*, 2015, **15**, 2389-2401.
 - 29 S. Tsuzuki, A. Wakisaka, T. Ono, T. Sonoda, Magnitude and Origin of the Attraction and Directionality of the Halogen Bonds of the Complexes of C₆F₅X and C₆H₅X (X=I, Br, Cl and F) with Pyridine. *Chem. Eur. J.*, 2012, **18**, 951-960.
 - 30 H. Torii, Correlation of the partial charge-transfer and covalent nature of halogen bonding with the THz and IR spectral changes. *Phys. Chem. Chem. Phys.*, 2019, **21**, 17118-17125.
 - 31 J. Wojcik, G. Holband, Variable-temperature studies of the 4-isopropylphenol crystal structure from X-ray diffraction. Comparison of thermal expansion and molecular dynamics with spectroscopic results. *J. Acta Crystallogr.*, 2002, **B58**, 684-689.
 - 32 M. H Palmer, M. Biczysko, K. A Peterson, C. S Stapleton, S. P Wells, Structural and Vibrational Properties of Iodopentafluorobenzene: A Combined Raman and Infrared Spectral and Theoretical Study. *J. Phys. Chem. A*, 2017, **121**, 7917-7924.
 - 33 A. E. S. Hardin, T. L. Ellington, S. T. Nguyen, A. L. Rheingold, G. S. Tschumper, D. L. Watkins, N. I. Hammer, A Raman Spectroscopic and Computational Study of New Aromatic Pyrimidine-Based Halogen Bond Acceptors *Inorganics*, 2019, **7**, 119.
 - 34 C. Adamo V. Barone, Toward reliable density functional methods without adjustable parameters: The PBE0 model *J. Chem. Phys.*, 1999, **110**, 6158-69.
 - 35 B. P. Pritchard, D. Altarawy, B. Didier, T. D. Gibson, T. L. Windus, A New Basis Set Exchange: An Open, Up-to-date Resource for the Molecular Sciences Community *J. Chem. Inf. Model.* 2019, **59**, 4814-4820,
 - 36 M. J. Frisch, G. W. Trucks, H. B. Schlegel, G. E. Scuseria, M. A. Robb, J. R. Cheeseman, G. Scalmani, V. Barone, B. Mennucci, G. A. Petersson, H. Nakatsuji, M. Caricato, X. Li, H. P. Hratchian, A. F. Izmaylov, J. Bloino, G. Zheng, J. L. Sonnenberg, M. Hada, M. Ehara, K. Toyota, R. Fukuda, J. Hasegawa, M. Ishida, T. Nakajima, Y. Honda, O. Kitao, H. Nakai, T. Vreven, J. A. Montgomery Jr., J. E. Peralta, F. Ogliaro, M. Bearpark, J. J. Heyd, E. Brothers, K. N. Kudin, V. N. Staroverov, R. Kobayashi, J. Normand, K. Raghavachari, A. Rendell, J. C. Burant, S. S. Iyengar, J. Tomasi, M. Cossi, N. Rega, J. M. Millam, M. Klene, J. E. Knox, J. B. Cross, V. Bakken, C. Adamo, J. Jaramillo, R. Gomperts, R. E. Stratmann, O. Yazyev, A. J. Austin, R. Cammi, C. Pomelli, J. W. Ochterski, R.L. Martin, K. Morokuma, V. G. Zakrzewski, G. A. Voth, P. Salvador, J.J. Dannenberg, S. Dapprich, A.D. Daniels, Farkas, J.B. Foresman, J.V. Ortiz, J. Cioslowski, D.J. Fox, Gaussian 09 Revision A.1, Gaussian Inc., Wallingford, CT, 2009.
 - 37 H. Jansen and P. Ros, Non-empirical molecular orbital calculations on the protonation of carbon monoxide, *Chem. Phys. Lett.*, 1969, **3**, 140-143.
 - 38 B. Liu and A. D. McLean, Accurate calculation of the attractive interaction of two ground state helium atoms, *J. Chem. Phys.*, 1973, **59**, 4557-4558.
 - 39 S. Boys, F. Bernardi, The calculation of small molecular interactions by the differences of separate total energies. Some procedures with reduced errors, *Mol. Phys.*, 1970, **19**, 553-566.
 - 40 Y-X. Lu, J-W Zou, Y-H Wang, Q-S. Yu, Theoretical investigations of the C-X/ π interactions between benzene and some model halocarbons, *Chemical Physics*, 2007, **334**, 1-7

- 41 K E. Riley, K. M. Merz, Insights into the Strength and Origin of Halogen Bonding: Halobenzene–Formaldehyde Dimer, *J. Phys. Chem. A*, 2007, **111**, 1688-1694.
- 42 S. Grimme, J. Antony, S. Ehrlich, H. Krieg, A consistent and accurate ab initio parameterization of density functional dispersion correction (DFT-D) for the 94 elements H-Pu, *J. Chem. Phys.*, 2010, **132**, 154104.
- 43 Y. Zhao, D. G. Truhlar, The M06 suite of density functionals for main group thermochemistry, thermochemical kinetics, noncovalent interactions, excited states, and transition elements: two new functionals and systematic testing of four M06-class functionals and 12 other functionals, *Theor. Chem. Acc.*, **120** (2008) 215-41.